Assembly of a Janus Composite Nanoparticle Optically Levitated in Vacuum

Jiangwei Yan(闫江伟)[1], Jiayu Feng(冯嘉煜)[1], Chenli Gao(高晨力)[1], Yuanbin Jin(靳元彬)[1], Zhengkun Fu(付正坤)[2], Zheng Han(韩拯)[1,3], Jing Zhang(张靖)[1*], and Xudong Yu(于旭东)[1*]

[1]*State Key Laboratory of Quantum Optics Technologies and Devices, Collaborative Innovation Center of Extreme Optics, Institute of Opto-Electronics, Shanxi University, Taiyuan 030006, China*
[2]*School of Physics and Information Technology, Shaanxi Normal University, Xi'an 710119, China*
[3]*Liaoning Academy of Materials, Shenyang 110167, China*

(Received 22 April 2025; accepted manuscript online 7 July 2025)

The optically levitated mechanical system in vacuum is a powerful platform in physics. It has been displaying more extensive application prospects. This paper presents an experimental study of optical levitation, identification, motion measurement, and assembly of two-species photoluminescence nanoparticles. A laser trapping array simultaneously levitates nitrogen-vacancy (NV) nanodiamonds and Yb^{3+}/Er^{3+}:$NaYF_4$ nanoparticles. The species of each nanoparticle can be individually identified by measuring the photoluminescence spectrum. We choose the single NV nanodiamond and Yb^{3+}/Er^{3+}:$NaYF_4$ nanoparticle and assemble them into a Janus composite nanoparticle, which integrates the merits of the two components. This work demonstrates the potential advantages of a hybrid optically levitated system. It provides a practicable scheme for the study of macroscopic quantum phenomena and precision measurement, thanks to the spin manipulation or spin-mechanical coupling of an NV diamond and by simultaneously implementing laser refrigeration to the Yb^{3+}/Er^{3+}:$NaYF_4$ nanoparticle in an optically levitated composite nanoparticle.

DOI: 10.1088/0256-307X/42/8/080403 CSTR: 32039.14.0256-307X.42.8.080403

1. Introduction. The vacuum optical levitation provides an important tool and testing ground for performing fundamental physics studies and precision measurements.[1–3] It has attracted much more attention and has become a burgeoning field. For an optically levitated single particle, significant advances have been made, such as quantum ground state cooling of the center-of-mass (CoM) motion at room temperature or using cryogenic technology,[4–7] observation of the libration oscillation and rotation around the axes of the solid body itself or in the transversal orbit,[8–14] as well as dynamical manipulation[15,16] and simultaneously cooling of multiple degrees of freedom in motions,[17,18] etc. Meanwhile, some theoretical studies have illustrated that the coupling of internal and external degrees of freedom can display rich physics.[19,20] For an optically levitated particle array, important progress includes light-induced coupling of two closed particles,[21–23] long-range interactions of two separated particles in an optical cavity,[24] sympathetically or separately cooling of two particles,[23,25] and levitation and assembly of multiple nanoparticles.[26] Moreover, the development of the quantum control technique will further promote the studies of macroscopic quantum phenomena and quantum sensors.[2,27]

From a material perspective, silica particles are usually utilized in the optically levitated system, especially in high vacuum, due to high phase-transition temperature and low absorption of the trapping laser in the optical communication region. However, manipulation of the internal degrees of freedom and coupling of internal and external degrees of freedom are difficult for homogeneous silica particles.[19,20] The diamond particle embedded with nitrogen-vacancy (NV) centers is believed to be a promising candidate because of the controllability with diverse internal and external operating techniques, the long coherence time of the electron spin at room temperature,[28] and high sensitivity to electric and magnetic fields.[29,30] Thanks to the spin-mechanical interaction of the levitated NV diamond particles, some experiments have realized spin-dependent torque and spin cooling of the libration,[31] angle locking of the crystalline axis,[32] spin control and Berry phase of electron spins in a rotating nanodiamond,[33] and so on. Nevertheless, the thermal effect and oxidation are essential obstacles to an optically levitated diamond particle in high vacuum.[34–36]

The thermal effect is universal in an optically levitated system in vacuum, which can make the trap unstable and limit the coherence of the quantum state and the sensitivity of the measurement.[37,38] The resultant oxidation for a diamond particle can also decrease its size and even burn it up.[39] Some attention turns to the laser refrigeration technique to reduce the internal temperature of an optically levitated nanomaterials, such as Yb^{3+}:YLF, Yb^{3+}:$NaYF_4$, and Yb^{3+}/Er^{3+}:$NaYF_4$ nanoparticles.[40–42] However, obtaining a long coherence time for the electron spin is difficult due to the complex components and structure of these rare-earth-doped materials. A Janus particle combines two or more different materials and can yield unique chemi-

*Corresponding authors. Email: jzhang74@sxu.edu.cn; jiance_yu@sxu.edu.cn
© 2025 Chinese Physical Society and IOP Publishing Ltd. All rights, including for text and data mining, AI training, and similar technologies, are reserved.

cal and physical properties relative to homogeneous particles due to the asymmetrical structure, which displays wide applications in biology, medical science, chemistry, and physics.[43,44] So far, the assembly and levitation of a Janus particle in an optically levitated system in vacuum have not been reported.

In this work, NV nanodiamonds and Yb^{3+}/Er^{3+}:$NaYF_4$ nanoparticles are simultaneously levitated by a trapping laser array in a vacuum chamber. The photoluminescence (PL) spectra of these nanoparticles are separately measured as fingerprints to discriminate the species of the nanoparticles. We manipulate the nanoparticles and assemble a nanodiamond with a Yb^{3+}/Er^{3+}:$NaYF_4$ nanoparticle into a Janus composite nanoparticle. The PL spectrum, motion signal, and scattering imaging of the Janus composite nanoparticle are measured when pressure is decreased. The minimum trapping pressure for the NV nanodiamond in the Janus composite nanoparticle is improved compared to the single NV nanodiamond, which relies mainly on the Yb^{3+}/Er^{3+}:$NaYF_4$ nanoparticle, because the heat transfer between the two components dramatically reduces the thermal effect of the nanodiamond and suppresses the oxidation process. This strategy sufficiently integrates the advantages of these two types of nanomaterials. It can also be applied to reduce the internal temperature of an optically levitated NV nanodiamond through heat transfer if laser refrigeration is implemented to the Yb^{3+}/Er^{3+}:$NaYF_4$ nanoparticle.[42]

2. Experiment Setup. In our recent experiment,[26] we realize a reconfigurable homogenous-nanoparticle array and perform the assembly on demand. In this experiment, we develop the system to levitate two species of PL nanoparticles, implement measurements to obtain the PL spectrum, motion signal, and scattering imaging of each nanoparticle, and perform the assembly. The experimental setup is shown in Fig. 1(a). Note that, in this experiment, all 1064 nm trapping lasers can excite Yb^{3+}/Er^{3+}:$NaYF_4$ nanoparticles.[45] Meanwhile, the 532 nm laser beam used to measure motion information can stimulate NV nanodiamonds. The 1064 nm and 532 nm lasers are all focused by an objective lens (OL, $NA = 0.95$, Nikon CF Plan 100×) in a vacuum chamber. Under the excitation of the 1064 nm and 532 nm laser beams, the NV nanodiamond and Yb^{3+}/Er^{3+}:$NaYF_4$ nanoparticle generate PL respectively. The back-emitted PL is collected by the OL and analyzed by a spectrometer (ANDOR, Shamrock 500i). A focus lens (L3) is mounted on the PL light path to converge them. An aperture installed on a translation stage is placed at the focus plane of L3 to select the PL and realize a spatially resolved detection of the different nanoparticles for the PL spectra. The PL is detected with a range from 650 to 1000 nm, which is determined by the bandwidth of the dichroic beam splitters DBS1 and DBS2. A removable mirror (RM) is placed on the path of the 532 nm back-scattered lights and excitation-detection laser to selectively perform scattering imaging or excitation and motion measurement.

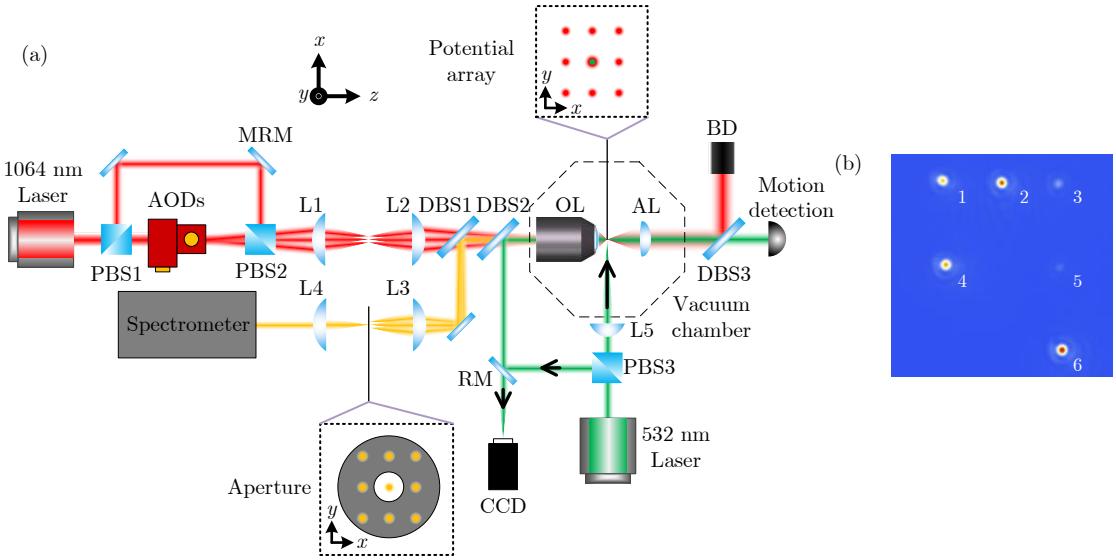

Fig. 1. (a) Schematic diagram of the experimental setup. A 1064 nm laser is divided into two parts. The frequency of one part is shifted by two orthogonally placed AODs to create a 3×3 trapping array[26] The other is used as an auxiliary beam. The powers of the trapping beams and the auxiliary beam are 100 mW and 200 mW, respectively. A 532 nm laser is separated to illuminate the nanoparticles in the array along the x axis and excite the NV nanodiamonds or detect the motion signal of the trapped nanoparticles along the z axis. The power of the illuminating beam and exciting beam are 500 μW and 5 mW, respectively. PBS1-3: polarized beam splitter, MRM: motor-driven reflective mirror, AODs: acousto-optic deflectors, L1-L5: lens, DBS1-3: dichroic beam splitter, OL: objective lens, AL: aspherical lens, BD: beam dump, RM: removable mirror, CCD: charge-coupled device. (b) Scattering imaging of a levitated nanoparticle array illuminated by a 532 nm laser and detected by the CCD. The species of the nanoparticles are identified by measuring their PL spectra. Particle 1 is a NV nanodiamond, particle 2 is a Yb^{3+}/Er^{3+}:$NaYF_4$ nanoparticle, and particle 6 is a composite particle consisting of two types of nanoparticles, which are possibly formed in the solution combination, atomization, or loading processes. Particles 3, 4, and 5 are nonluminescent contaminants.

3. Materials. The commercial NV nanodiamonds (Adamas Nanotechnologies, ND-NV-40nm-Hi) with a nominal diameter of 40 nm are utilized in the experiment. The Yb^{3+}/Er^{3+}:$NaYF_4$ nanoparticles are homemade and synthesized through the hydrothermal method. They are near-spherical with a diameter of about 200 nm and have a hexagonal phase. The doping concentrations of the Yb^{3+} and Er^{3+} ions are 20% and 2%, respectively. Both nanoparticles are water-soluble. Their solutions are mixed with a number density ratio of 1 : 1 and sonicated to make the nanoparticles monodispersed. The monodispersed nanoparticles are then dispersed into the vacuum chamber by an ultrasonic nebulizer and loaded into the trapping laser array.

The energy level diagram of a diamond NV center is shown in Fig. 2(a). The NV centers are optically excited to the high energy level (^{3}E) by the 532 nm laser, which return to the ground state with a red-shifted PL or through nonradiative decays. Figure 2(b) displays the energy levels and transitions of Yb^{3+} and Er^{3+} ions in the $NaYF_4$ nanoparticles. The Yb^{3+} ions in the ground state are excited to the $^2F_{5/2}$ state by the 1064 nm laser. The mismatch between the transition and the laser is compensated by the internal phonons of the nanoparticle. The energy of the excited state Yb^{3+} ions can be transferred to the Er^{3+} ions, leading to excitation transitions of the Er^{3+} ions.[42] After energy transfer, the Yb^{3+} ions return to the ground state. The nonradiative relaxation processes of the Er^{3+} ions in the exited state occur. Meanwhile, Er^{3+} ions in the excited states of $^2H_{11/2}$, $^4S_{3/2}$, and $^4F_{9/2}$, can drop to the ground state through radiative decays.

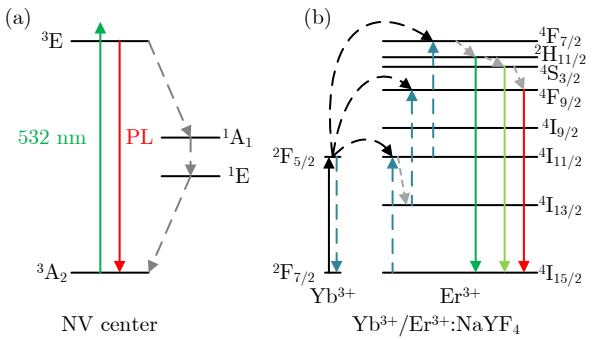

Fig. 2. Schematic diagram of the energy levels. (a) Energy level diagram of a diamond NV center. The 532 nm laser (green arrow) excites the NV centers. The red solid and gray dashed arrows represent radiative and nonradiative decays. (b) Energy levels of Yb^{3+} and Er^{3+} ions in a $NaYF_4$ nanoparticle. The transition of Yb^{3+} ions from the ground state to $^2F_{5/2}$ is denoted by the black solid arrow under the excitation of the 1064 nm laser with the assistance of the internal phonons of the nanoparticle. The black dashed arrows represent the energy transfer from Yb^{3+} ions to Er^{3+} ions. In these processes, the Er^{3+} ions can be excited to high energy levels, and the Yb^{3+} ions would return to the ground state after the energy transfer, denoted by the blue dashed arrows. The gray dashed arrows illustrate the nonradiative relaxations of Er^{3+} ions. The deep green, light green, and red solid arrows denote the radiative decays.

4. Results and Discussion. Figure 1(b) shows the scattering imaging of six randomly captured nanoparticles at atmospheric pressure. By separately measuring their PL spectra, we confirm their species. We remove the contaminants with the composite particle and leave particles 1 and 2, and then start the pump to evacuate the vacuum chamber and measure the PL spectra and scattering imaging of these two nanoparticles. Figures 3(a)–3(f) illustrate the PL spectrum, total PL intensity, scattering imaging, and total scattering intensity of these two nanoparticles at different pressures. The CoM motion signals of the two nanoparticles are detected by a motion detection system, as depicted in Figs. 3(g) and 3(h).

The PL spectrum and total PL intensity of the NV nanodiamond decrease as the pressure decreases, as shown in Figs. 3(b) and 3(c). The reason comes from three aspects. One is the increase in internal temperature due to the absorption of lights and attenuation of heat dissipation with the pressure reduction, which enhances the nonradiative transitions and weakens the radiative transition. The other is the size reduction caused by oxidation in the residual air in the vacuum chamber.[39] Meanwhile, the size reduction decreases the scattering intensity of the NV nanodiamond, as shown in Figs. 3(e) and 3(f). The third is the photo-induced ionization in the case of simultaneous presences of 532 nm and 1064 nm lasers.[46] Figure 3(h) shows the power spectrum densities (PSDs) of the CoM motions of the NV nanodiamond along the x, y, and z axes at 80 mbar. These CoM motion signals are broad, which are associated with large damping rates. The external degrees of freedom can be coupled with the internal degrees of freedom induced by the collisions of the nanoparticles and residual air molecules. At high internal temperature, energy exchange between nanoparticles and air molecules becomes violent and results in the loss of nanoparticles.[39] In our experiment, the loss pressure for nanodiamonds is in the range of about 60 to 100 mbar.

In contrast, the PL spectrum and the total PL intensity of the Yb^{3+}/Er^{3+}:$NaYF_4$ nanoparticle increase as the pressure decreases, as shown in Figs. 3(a) and 3(c). The absorption of light raises the internal temperature of the Yb^{3+}/Er^{3+}:$NaYF_4$ nanoparticle during the pressure reduction process, which is the same as that of the NV nanodiamond, as discussed above. On the contrary, the increase in phonon number enhances the excitation transition of Yb^{3+} ions and the energy transfer from Yb^{3+} to Er^{+3} ions; therefore, it boosts the PL intensity of the Yb^{3+}/Er^{3+}:$NaYF_4$ nanoparticle.[47] The oxidation effect can also decrease the size and simultaneously reduce the scattering intensity of the Yb^{3+}/Er^{3+}:$NaYF_4$ nanoparticle. The scattering imaging and total scattering intensity at different pressures are shown in Figs. 3(d) and 3(f). Figure 3(g) illustrates the CoM motion signals of the Yb^{3+}/Er^{3+}:$NaYF_4$ nanoparticle along the x, y, and z axes at 30 mbar. Due to the larger scale and lower measurement pressure for the Yb^{3+}/Er^{3+}:$NaYF_4$ nanoparticle, these CoM motion signals are narrower than those of the NV nanodiamond. The loss pressure range for the Yb^{3+}/Er^{3+}:$NaYF_4$ nanoparticle is about 15 to 30 mbar in this experiment.

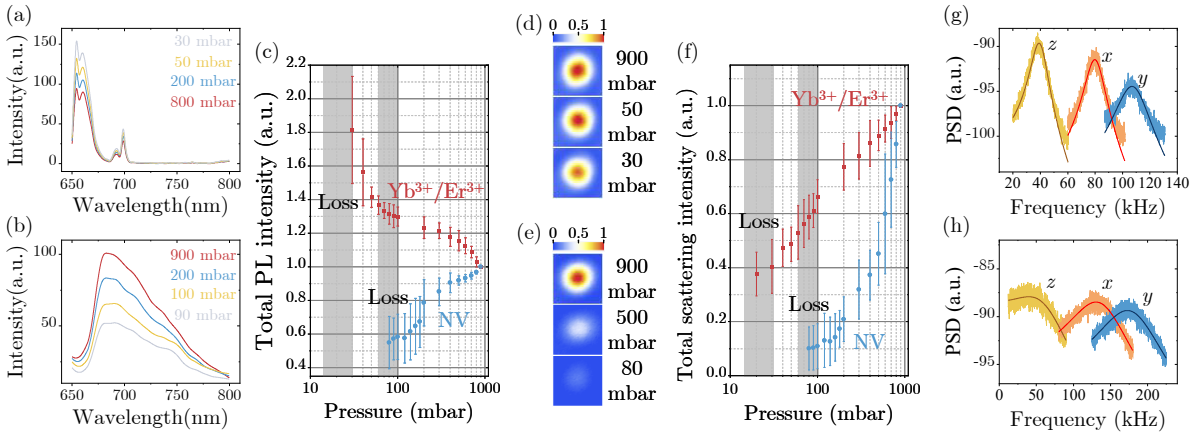

Fig. 3. (a) PL spectra of a single Yb^{3+}/Er^{3+}:$NaYF_4$ nanoparticle individually stimulated by the 1064 nm laser at different pressures. (b) PL spectra of a single NV nanodiamond stimulated by the 532 nm laser at different pressures. (c) Total PL intensities of the NV nanodiamond and Yb^{3+}/Er^{3+}:$NaYF_4$ nanoparticle versus the pressure. The total PL intensity is achieved by integrating the PL spectrum of a single-species nanoparticle from 650 nm to 800 nm. (d) and (e) Scattering imaging of these two nanoparticles illuminated by a 532 nm laser at different pressures. (f) Total scattering intensity changes of these two nanoparticles versus the pressure. The total scattering intensity corresponds to the scattering intensity integral on the CCD. (g) and (h) PSD of the CoM motion of the Yb^{3+}/Er^{3+}:$NaYF_4$ nanoparticle and NV nanodiamond at 30 mbar and 80 mbar, respectively; the smooth dark curves are the fittings of the motion signals. The measurement time of each PL spectrum is about 20 seconds. The exposure time of the CCD is set to 0.5 seconds to achieve the scattering imaging. The air pressure is decreased slowly to perform all the measurements.

The upconversion PL, thanks to the energy transfer between the two different ions, can lower the internal phonon number of the Yb^{3+}/Er^{3+}:$NaYF_4$ nanoparticle and make the internal temperature drop.[42] However, due to the mismatches of doping concentrations for the two ions, the wavelength of the excitation laser, and the transition of the Yb^{3+} ion, as well as the absorption of impurities in the $NaYF_4$ nanoparticle, especially in a strong trapping laser field, the heating effect is dominated and refrigeration is not observed. Another option to decrease the internal temperature is to use a single Yb^{3+} ions-doped $NaYF_4$ nanoparticle stimulated by a 1020 nm laser.[41] For a purer material simultaneously satisfying the match conditions of ion concentration and excitation-transition, the radiations of shorter wavelength lights than the excitation laser can effectively carry away the additional energy from the crystal phonons. Thus, the internal temperature of the material can be decreased, which is called anti-Stokes cooling.[40,41] In future experimental studies, the corresponding optimized schemes with the optimized materials will be adopted.

After the above measurements, we recapture the two types of nanoparticles in the optically trapping array and choose the single NV nanodiamond and Yb^{3+}/Er^{3+}:$NaYF_4$ nanoparticle. Next, by controlling the auxiliary beam, we move the NV nanodiamond and the Yb^{3+}/Er^{3+}:$NaYF_4$ nanoparticle into a single trap and stick them together to form a Janus composite nanoparticle. The PL spectrum of the Janus composite nanoparticle coexcited by the 1064 nm and 532 nm lasers is measured at atmospheric pressure, as shown by the yellow curve in the inset of Fig. 4(a). The red curve is the result of individual excitation by the 1064 nm trapping laser, and the blue curve is derived from the subtraction of these two signals, which is consistent with the PL spectrum of a single NV nanodiamond. After the assembly, we decrease the pressure. The host graph in Fig. 4(a) illustrates the total PL intensity of the two components in the Janus composite nanoparticle at different pressures. The total PL intensity changes of the two components with pressure are opposite and have roughly similar trend properties to the individual nanoparticles. However, unlike the individual NV nanodiamond, the PL spectrum of the NV nanodiamond component in the Janus composite nanoparticle can be observed at 40 mbar until the Janus composite nanoparticle is lost. Figure 4(b) corresponds to the total scattering intensity of the Janus composite nanoparticle at different pressures. As pressure decreases, the total scattering intensity gradually reduces as a result of oxidation of the two nanoparticles. The changes in PL spectra for the two components and scattering intensity of the Janus composite nanoparticle are caused by the inducements discussed above, simultaneously superposed with the heat transfer between the two nanoparticles. At 40 mbar, we measured the CoM motion signals of the Janus composite nanoparticle, as shown in Fig. 4(c), which can be used to confirm the success of assembly.[26] The loss pressure range of the Janus composite nanoparticle is about 15 to 40 mbar. It is mainly dependent on the Yb^{3+}/Er^{3+}:$NaYF_4$ nanoparticle due to its relatively large volume and the resulting large thermal capacity and is slightly different from that of the single Yb^{3+}/Er^{3+}:$NaYF_4$ nanoparticles owing to the relatively small volume and higher internal temperature of the NV nanodiamond component. Compared to the individual NV nanodiamond, the minimum trapping pressure of the nanodiamond in the Janus composite nanoparticle is significantly improved by means of heat transfer from the NV nanodiamond to the Yb^{3+}/Er^{3+}:$NaYF_4$ nanoparticle.[48]

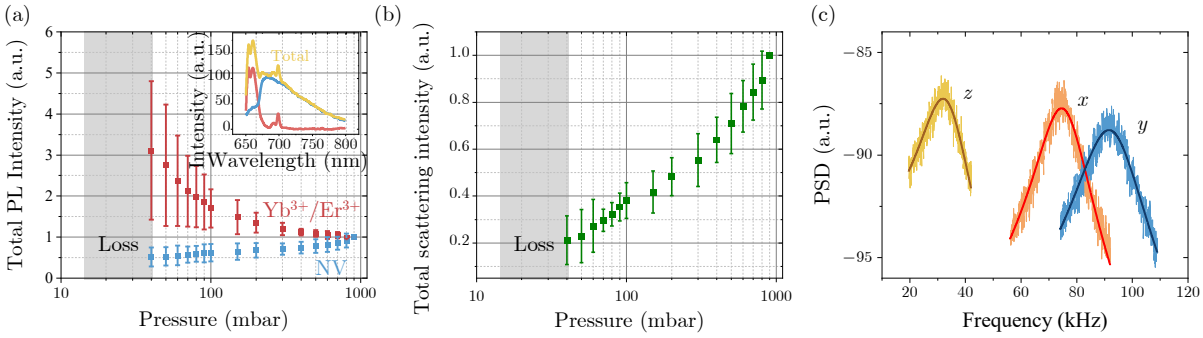

Fig. 4. (a) Total PL intensities of the two components in the Janus composite nanoparticle versus the pressure. The inset is the PL spectra of the Janus composite nanoparticle at atmospheric pressure. The yellow curve is the PL spectrum of the composite nanoparticle excited by the 1064 nm and 532 nm lasers. The red curve is the PL spectrum individually excited by the 1064 nm laser. The blue curve is a subtraction result of the yellow and red curves. In the host graph, the red squares and blue circles correspond to the total PL intensities of the two components, which are separately obtained through the integrals of the individual component PL spectra over the range from 650 nm to 800 nm at different pressures. (b) Total scattering intensity of the Janus composite nanoparticle versus the pressure. (c) CoM motion PSDs of the Janus composite nanoparticle at 40 mbar; the smooth dark curves are the fittings of the motion signals. The measurement time and the change speed of air pressure are similar to those of Fig. 3.

In addition, these results in our experiment are different from the other works using a type of PL particles.[39,42] This difference arises from two reasons. One is the difference in particles, such as the impurity level. The other is the relatively high power of the trapping beams in our experiment, which enhances the thermal effects for observing and comparing changes in the PL spectrum and scattering.

5. Conclusion. In conclusion, we developed a technique of simultaneous levitation, identification, motion measurement, and assembly of two-species PL nanoparticles in a vacuum. Each nanoparticle can be distinguished by measuring the PL spectrum, which greatly benefits from the characterized PL spectral fingerprints. This work expands the studies of vacuum optical levitation into the field of interaction and assembly in a multi-species particle array. Moreover, the assembled Janus composite nanoparticle can integrate the advantages of both types of nanoparticles. Its minimum trapping pressure relies on the Yb^{3+}/Er^{3+}:$NaYF_4$ nanoparticle. Heat transfer between two nanoparticles suppresses the heating effect and oxidation of the NV nanodiamond and improves its performance in a vacuum. Meanwhile, Yb^{3+} and Er^{3+} ions doped $NaYF_4$ is a potential material to realize laser refrigeration.[42] A composite nanoparticle containing the Yb^{3+}/Er^{3+}:$NaYF_4$ nanoparticle or other laser-refrigerating nanomaterials can be expected to achieve joint refrigeration through heat transfer.[48] This is crucial for studies of macroscopic quantum states and precision measurements through spin control or spin-mechanical coupling of an NV nanodiamond.

Acknowledgements. This work was supported in part by the National Natural Science Foundation of China (Grant Nos. 61975101, 11234008, 11361161002, and 6157-1276).

References

[1] Millen J, Monteiro T S, Pettit R, and Vamivakas A N 2020 *Rep. Prog. Phys.* **83** 026401
[2] Gonzalez-Ballestero C, Aspelmeyer M, Novotny L, Quidant R, and Romero-Isart O 2021 *Science* **374** eabg3027
[3] Winstone G, Grinin A, Bhattacharya M, Geraci A A, Li T C, Pauzauskie P J, and Vamivakas N 2024 arXiv:2307.11858
[4] Delić U, Reisenbauer M, Dare K, Grass D, Vuletić V, Kiesel N, and Aspelmeyer M 2020 *Science* **367** 892
[5] Magrini L, Rosenzweig P, Bach C, Deutschmann-Olek A, Hofer S G, Hong S, Kiesel N, Kugi A, and Aspelmeyer M 2021 *Nature* **595** 373
[6] Tebbenjohanns F, Mattana M L, Rossi M, Frimmer M, and Novotny L 2021 *Nature* **595** 378
[7] Piotrowski J, Windey D, Vijayan J, Gonzalez-Ballestero C, de los Ríos Sommer A, Meyer N, Quidant R, Romero-Isart O, Reimann R, and Novotny L 2023 *Nat. Phys.* **19** 1009
[8] Hoang T M, Ma Y, Ahn J, Bang J, Robicheaux F, Yin Z Q, and Li T C 2016 *Phys. Rev. Lett.* **117** 123604
[9] Kuhn S, Kosloff A, Stickler B A, Patolsky F, Hornberger K, Arndt M, and Millen J 2017 *Optica* **4** 356
[10] Reimann R, Doderer M, Hebestreit E, Diehl R, Frimmer M, Windey D, Tebbenjohanns F, and Novotny L 2018 *Phys. Rev. Lett.* **121** 033602
[11] Ahn J, Xu Z J, Bang J, Deng Y H, Hoang T M, Han Q K, Ma R M, and Li T C 2018 *Phys. Rev. Lett.* **121** 033603
[12] Monteiro F, Ghosh S, van Assendelft E C, and Moore D C 2018 *Phys. Rev. A* **97** 051802
[13] Jin Y B, Yan J W, Rahman S J, Li J, Yu X D, and Zhang J 2021 *Photon. Res.* **9** 1344
[14] Hu Y H, Kingsley-Smith J J, Nikkhou M, Sabin J A, Rodríguez-Fortuño F J, Xu X H, and Millen J 2023 *Nat. Commun.* **14** 2638
[15] Zielínska J A, van der Laan F, Norrman A, Rimlinger M, Reimann R, Novotny L, and Frimmer M 2023 *Phys. Rev. Lett.* **130** 203603
[16] Zielińska J A, van der Laan F, Norrman A, Reimann R, Frimmer M, and Novotny L 2024 *Phys. Rev. Lett.* **132** 253601
[17] Bang J, Seberson T, Ju P, Ahn J, Xu Z J, Gao X Y, Robicheaux F, and Li T C 2020 *Phys. Rev. Res.* **2** 043054
[18] Pontin A, Fu H, Toroš M, Monteiro T S, and Barker P F 2023 *Nat. Phys.* **19** 1003
[19] Yin Z Q, Li T C, Zhang X, and Duan L M 2013 *Phys. Rev. A* **88** 033614
[20] Scala M, Kim M S, Morley G W, Barker P F, and Bose S 2013 *Phys. Rev. Lett.* **111** 180403
[21] Arita Y, Wright E M, and Dholakia K 2018 *Optica* **5** 910

[22] Rieser J, Ciampini M A, Rudolph H, Kiesel N, Hornberger K, Stickler B A, Aspelmeyer M, and Delić U 2022 *Science* **377** 987

[23] Arita Y, Bruce G D, Wright E M, Simpson S H, Zemánek P, and Dholakia K 2022 *Optica* **9** 1000

[24] Vijayan J, Piotrowski J, Gonzalez-Ballestero C, Weber K, Romero-Isart O, and Novotny L 2024 *Nat. Phys.* **20** 859

[25] Vijayan J, Zhang Z, Piotrowski J, Windey D, van der Laan F, Frimmer M, and Novotny L 2023 *Nat. Nanotechnol.* **18** 49

[26] Yan J W, Yu X D, Han Z V, Li T C, and Zhang J 2023 *Photon. Res.* **11** 600

[27] Moore D C and Geraci A A 2021 *Quantum Sci. Technol.* **6** 014008

[28] Bar-Gill N, Pham L M, Jarmola A, Budker D, and Walsworth R L 2013 *Nat. Commun.* **4** 1743

[29] Hall L T, Cole J H, Hill C D, and Hollenberg L C L 2009 *Phys. Rev. Lett.* **103** 220802

[30] Dolde F, Fedder H, Doherty M W, Nöbauer T, Rempp F, Balasubramanian G, Wolf T, Reinhard F, Hollenberg L C L, Jelezko F, and Wrachtrup J 2011 *Nat. Phys.* **7** 459

[31] Delord T, Huillery P, Nicolas L, and Hétet G 2020 *Nature* **580** 56

[32] Perdriat M, Huillery P, Pellet-Mary C, and Hétet G 2022 *Phys. Rev. Lett.* **128** 117203

[33] Jin Y, Shen K, Ju P, Gao X, Zu C, Grine A J, and Li T 2024 *Nat. Commun.* **15** 5063

[34] Neukirch L P, von Haartman E, Rosenholm J M, and Nick Vamivakas A 2015 *Nat. Photonics* **9** 653

[35] Delord T, Nicolas L, Bodini M, and Hétet G 2017 *Appl. Phys. Lett.* **111** 013101

[36] Rahman A T M A, Frangeskou A C, Kim M S, Bose S, Morley G W, and Barker P F 2016 *Sci. Rep.* **6** 21633

[37] Lu D, Gámez F, and Haro-González P 2021 *Micromachines* **12** 954

[38] Hu M, Li N, Fu Z, Yang J, Zhang Y, Li W, Cai H, and Hu H 2023 *Opt. Commun.* **546** 129784

[39] Hoang T M, Ahn J, Bang J, and Li T C 2016 *Nat. Commun.* **7** 12250

[40] Rahman A T M A and Barker P F 2017 *Nat. Photonics* **11** 634

[41] Luntz-Martin D R, Felsted R G, Dadras S, Pauzauskie P J, and Vamivakas A N 2021 *Opt. Lett.* **46** 3797

[42] Zhang B, Guo X, Yu X, Xiao Y, Fu Z, Zhang Z, and Zheng H 2023 *Phys. Rev. A* **108** 033503

[43] Rahiminezhad Z, Tamaddon A M, Borandeh S, and Abolmaali S S 2020 *Appl. Mater. Today* **18** 100513

[44] Zhang T, Lyu D, Xu W, Feng X, Ni R, and Wang Y 2023 *Nat. Commun.* **14** 8494

[45] Li Z H, Hudry D, Heid R, Said A H, Le M D, Popescu R, Gerthsen D, Merz M, Krämer K W, Busko D, Howard I A, Richards B S, and Weber F 2020 *Phys. Rev. B* **102** 165409

[46] Aslam N, Waldherr G, Neumann P, Jelezko F, and Wrachtrup J 2013 *New J. Phys.* **15** 013064

[47] Yan L, Huang J S, An Z C, Zhang Q Y, and Zhou B 2022 *Nano Lett.* **22** 7042

[48] Zhu C Y and Li Z Y 2021 *Int. J. Heat Mass Transf.* **167** 120723